Scanning Microscopy Vol. 13, No. 1, 1999 (Pages 7-22) 0891-703599$5.00+.25
Scanning Microscopy International, Chicago (AMF O'Hare), IL 60666 USA

IMAGING OF SPECIMENS AT OPTIMIZED LOW AND VERY LOW ENERGIES IN SCANNING ELECTRON MICROSCOPY

Ilona Müllerová

Institute of Scientific Instruments, Academy of Sciences of the Czech Republic, Brno, Czech Republic

(Received for publication April 4, 1998 and in revised form August 3, 1998)

Abstract

A modern trend toward low electron energies in scanning electron microscopy (SEM), characterised by lowering the acceleration voltages in low voltage SEM (LVSEM) or by utilising a retarding-field optical element in low energy SEM (LESEM), makes the energy range where new contrasts appear accessible. This range is further extended by a cathode-lens equipped scanning low energy electron microscope (SLEEM) which achieves nearly constant spatial resolution throughout the energy scale. This enables one to optimise freely the electron beam energy according to the task. At low energies, classes of image contrast exist that make visible particular specimen data most effectively or even exclusively within certain energy intervals or at certain energy values only. Some contrasts are well understood and can already be utilised for practical surface examinations but others are not yet reliably explained and complementary experiments are needed.

Key Words: Contrast mechanisms, low electron energies, scanning electron microscope.

*Address for correspondence:
Ilona Müllerová
Institute of Scientific Instruments
Academy of Sciences of the Czech Republic
Královopolská 147, 612 64 Brno, Czech Republic
Telephone number: +420-5-41514300
FAX Number: : +420-5-41514402
E-mail: ilona@isibrno.cz

Introduction

The conventional scanning electron microscope (SEM) usually operates at energy around 15 keV, where it is possible to find an optimum from the point of view of sufficient brightness of the primary electron beam, good resolution and a reasonable interaction volume from which information arises about the specimen. In other words, the SEM energies are traditionally chosen mostly from the point of view of the microscope column performance.

Even thirty years before the first commercial SEM was made available on the market, some advantages of the SEM operated at low electron energies (below 5 keV) were recognised (Knoll, 1935). A similarly long period of instrument development was needed to develop low energy SEM for routine exploitations. Nowadays, the world SEM producers offer instruments with a resolution of several nm at energies as low as about 200-500 eV. To get such a good resolution at low energies, much progress had to be made in the development of field emission guns with high brightness and small electron energy spread, of the electron optical elements for the formation of the primary electron beam of a small diameter, and of the detection of signal electrons. Ultrahigh vacuum (UHV) environment is necessary for the field emission gun, as well as for the specimen chamber, if the real surfaces are to be studied at a high surface sensitivity. For these instruments the acronym LVSEM (Low Voltage SEM) is usually used, as the acceleration voltage in the SEM gun is actually low.

The main advantages connected with decreasing energy are as follows. The beam interaction volume in the specimen diminishes significantly, so that the information acquired is much more surface sensitive. Moreover, the total electron yield increases and even exceeds unit level. Consequently, it is possible to find primary electron energies at which the surface potential can be stabilised and insulators without any coating can be observed (Thornley, 1960).

The next effort in the SEM development was directed to very low energies, even down to mirror microscopy where the impacting beam energy is nearly zero. A highly attractive model is the Low Energy Electron Microscope (LEEM) (Bauer, 1994), i.e., the emission electron microscope where the specimen emission is excited after impact of a coherent

planar electron wave. As usual in emission microscopes, the specimen is part of the cathode lens and a strong uniform field between the specimen and a suitable anode extracts and accelerates the signal electrons, thus securing a resolution which is surprisingly good, given the circumstances. Under an electron energy of tens and units of eV, new contrast mechanisms arise that are related to the electron diffraction and to the energy band structure of the specimen.

During the last three decades, many attempts were made to utilise retarding-field optical elements in SEM for purposes of improving the resolution at low energies. These attempts are summarised in the review paper of Müllerová and Lenc (1992a). Some of them were very promising but none were advanced enough to bring this version of SEM into routine as the Low Energy SEM (LESEM) method. LESEM can be understood as the SEM with low electron energies created as a difference between two relatively high voltages, those of the gun cathode and of the retarding-field element. For a few years, the first commercial LESEM has been marketed with so called "Gemini objective lens" (Frosien *et al*., 1989; Martin *et al*., 1994).

As a special retarding-field element the cathode lens, identical with that used in LEEM and other emission microscopes, was introduced into the SEM as a part of its objective lens. The aim was to achieve a high resolution down to very low energies. Full utilisation of the cathode lens in the SEM was experimentally proved by Müllerová and Lenc (1992b), and the theory of the cathode lens taking into account both the uniform field and the anode opening field and particularly of the combination of the cathode lens with the necessary focusing lens was developed (Lenc and Müllerová, 1992a,b). Preliminary image series were published which exhibited a consistent quality throughout the energy scale down to a nearly zero landing energy of electrons (Müllerová and Frank, 1993), and the basic imaging parameters were quantitatively verified (Müllerová and Frank, 1994). The cathode lens equipped SEM is capable of holding the image resolution near to the nominal one, down to the lowest energies, as is the case in LEEM. The acronym SLEEM (Scanning LEEM) is therefore suitable for this method and the LEEM family of contrasts is available in principle. The first successful attempt has already been made (Frank and Müllerová, 1997).

For the SLEEM observation, the full energy scale is easily accessible and in principle no restrictions arise with regard to the instrument performance (although in practice, the UHV design, specimen preparation, precautions against external spurious fields, etc., raise the appropriate apparatus into the category of a sophisticated instrument). This leaves one free to choose the electron energy exclusively on the basis of the phenomenon under study. In doing this, one can observe some general trends concerning the behaviour of the traditional SEM contrast mechanisms at low energies that extend the usefulness of this tool. In addition, some entirely new contrast mechanisms appear which either take place below a certain energy level (although usually not a sharply defined one) or which are limited to a finite energy interval. Some of these contrasts are understandable; they were even expected in advance and the advantage is that they are obtained at a high resolution. The corresponding images can be directly compared with conventional SEM images taken by using secondary electron (SE) and backscattered electron (BSE) signals at high energies. Nevertheless, as the collection of experience in very low energy microscopy started not long ago, some contrasts are not reliably understood as yet and a comparison with complementary observation modes (like Auger or photoelectron microscopy) is needed (El Gomati *et al*., 1997).

This paper presents some observations made on various structures by using low and very low energy electrons characterised by features that are available in a certain energy interval only. These can be considered as candidates for tasks solvable at "optimised" SEM energies. For most of the items included in this review, some white spots remain in their interpretation while for others, only hypothetical explanations are available.

Electron Optics of the Low and Very Low Energy SEM

The main problem connected with the LVSEM design is to maintain the spatial resolution at a level, not too far from the nominal resolution level, which at present lies in the low nanometer range. It is customary to express the SEM image resolution in terms of the primary beam spot size. This approach avoids consideration of the specimen influence, which is difficult owing to the specimen diversity but necessary in any rigorous treatment. In fact, the specimen forms a part of the Instrument Response Function (IRF) because the whole interaction volume contributes to the pixel intensity. It is interesting to find that when electron probe spreading within the specimen is taken into account in order to calculate the "real" SEM resolution, the result is crucially dependent on the class of the resolution criteria chosen (Frank, 1996a). While an integral criterion, based e.g., on a certain encircled-energy value or on the root-mean-square distance of the emitted electron brings some optimum landing energy of electrons for the minimum resolution, any criteria based on a defined drop in the IRF amplitude brings nothing new with respect to the spot size-based results. The optimum electron energy for integral resolution criteria lies in the dependence on the mean atomic number, around 1 keV for SLEEM and LESEM and increases up to a few keV for lower resolution SEMs (Frank, 1996b). On the other hand, the IRF amplitude - connected criteria, like the Rayleigh one, reveal the specimen contribution as negligible, i.e., so widely smeared that it can be

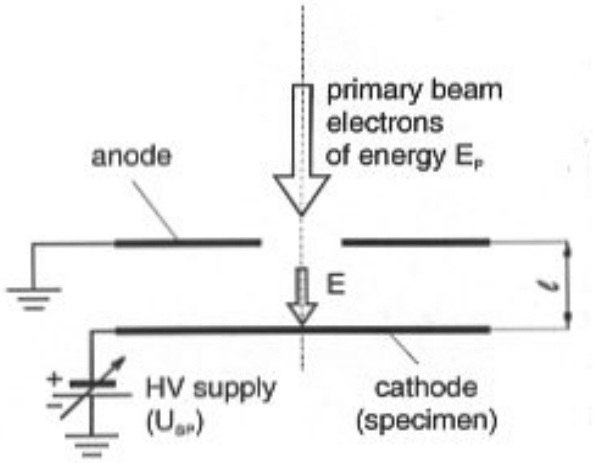

Figure 1. Schematic arrangement of the cathode lens.

considered disappearing within the electronically correctable quasi-homogeneous image background. This encourages us to restrict ourselves to spot size-based considerations.

An approximation of the total spot size of the primary beam d_T can be written as a sum of squares of the gaussian spot size d_G (diameter of a demagnified source) and spherical (d_S), chromatic (d_C) and diffraction (d_l) aberration discs:

$$d_T^2 = d_G^2 + d_S^2 + d_c^2 + d_\lambda^2 \tag{1}$$

$$d_G = \sqrt{\frac{4 I_P}{B\pi^2\alpha^2}}\,; \quad d_S = 0.5 S\alpha^3$$

$$d_C = C\frac{\Delta E}{E}\alpha; \quad d_\lambda = \frac{0.6\lambda}{\alpha} \tag{2}$$

I_P is the current in the probe, B is the source brightness, E is the beam energy, a is the aperture angle, DE is the energy spread of primary beam electrons, S and C are the spherical and chromatic aberration coefficients of the probe forming lens, respectively, and l is the electron wavelength.

The goal of the design of the SEM is to have a small spot size of the primary beam d_T with a sufficient current. The diameters of the individual aberration discs are directly or indirectly proportional to the aperture angle a, and therefore it is possible to find an optimum value. We can see from the above equations that we need to have an electron source of high brightness and small energy spread DE and the coefficients of spherical and chromatic aberration (S and C) as small as possible. To have a small spot size d_T with a sufficient current is even more complicated in the case of LVSEM. When the energy E decreases by several orders of magnitude, the dimensions d_G, d_C and d_l increase, and therefore resolution becomes worse. To operate at low energies, a probe-forming lens of extremely small aberration coefficients has to be designed and a source of high brightness and small energy spread has to be used. A lot of work had to be done on the design of the small aberration lenses for LVSEM and several overviews of the topic are available from Beck *et al*. (1995), Plies (1994) and Müllerová and Lenc (1992a).

In order to make the whole range of electron impact energies available, we would best need the spot size independent of the electron energy. Let us for the moment simplify Equation (1) by neglecting the first term so that only aberration induced enlargements of the spot size are considered. Suppose we vary the electron energy E to get a constant resolution d_T. This can be achieved when all d_S, d_C and d_l also keep constant values. Then we get from the expression for d_l the optimum angular aperture $a \propto E^{-1/2}$ (because $1 \propto E^{-1/2}$). Substituting this into expressions for d_S and d_C, we find them both proportional to $E^{-3/2}$ so that these aberration discs will not expand at low energies when relations $C \propto E^{3/2}$ and $S \propto E^{3/2}$ are satisfied. Such proportionality is unrealistic for normal objective lenses, and instead C and S are independent of the energy which makes d_T strongly energy dependent. Nevertheless, this does not hold for immersion electrostatic lenses, e.g., for the cathode lens.

The cathode lens was generally used as an objective lens of emission microscopes (Möllenstedt and Lenz, 1963). It is usually formed by a cathode held at a negative potential and by an anode at ground potential (Fig. 1). In an emission microscope, the specimen forms the cathode. This is the main component of a LEEM and when it is to be used in a SEM to provide for the SLEEM method, the cathode lens is inserted below the original focusing objective lens. Primary beam electrons of a relatively high energy E which is usually used in SEM, say about 10 to 20 keV, are decelerated to the specimen by a negative potential at the specimen (U_{SP}) which is finely adjustable. The aberration coefficients of the cathode lens can be approximately given as $S_{CL} \cong -C_{CL} \cong l\,(E/E_P)$, for $E << E_P$. E is an energy with which electrons strike the specimen, E_P is the primary beam energy and l is the distance between the anode and cathode of the cathode lens. The aberration coefficient decreases as the landing energy falls for a fixed l and primary beam energy E_P, which is what we need in order to achieve the small spot size at low energies. Because the cathode lens forms only a virtual image, a focusing lens has to be used. More details about the cathode lens and about the cathode lens in combination with the focusing lens can be found in (Lenc and Müllerová, 1992a,b). The effective energy dependence of the aberration coefficients is linear so that a "majority" of the desired $E^{3/2}$ proportionality is available here. Thus,

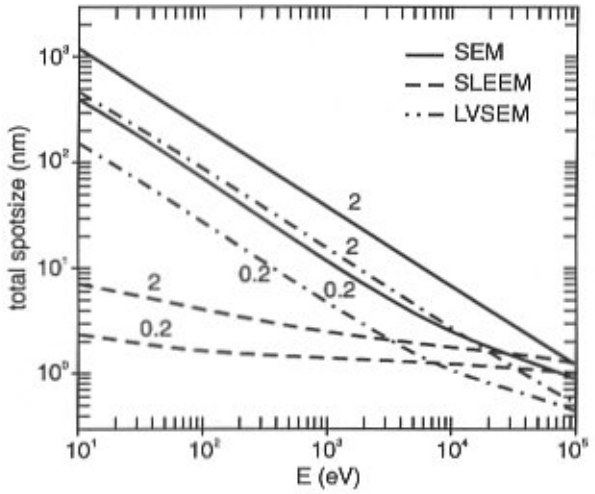

Figure 2. Spatial resolution (total spot size d_T) as a function of the electron landing energy according to the exact equations published by Lenc and Müllerová (1992b) and for an optimum angular aperture. The aberration coefficients of the magnetic focusing lens are C^m = 15mm and S^m = 30mm for SLEEM (cathode lens is used) and SEM (without cathode lens). C^m = 2.5 mm and S^m = 1.9 mm for LVSEM without cathode lens. The electron energy spread is 2 eV and 0.2 eV, as labelled.

---

although the absolute value of the SLEEM resolution is fully dependent on the objective lens quality, the resolution-to-energy dependence is very weak. Any SEM may be adapted for SLEEM by introducing the cathode lens, below a certain energy it exceeds even the best LVSEM in resolution. The LESEM designs lie in principle between both these types and the same is true for their parameters.

The dependence of the total spot size d_T as a function of the landing energy is shown in Figure 2. The calculations were done according to exact equations published by Lenc and Müllerová (1992b). The figure compares all three types described above and demonstrates the principal distinction of SLEEM, which is the only type capable of producing the micrographs with a quality consistent throughout the full energy scale.

Two possible experimental arrangements (Müllerová and Frank, 1993, 1994) are given in Figures 3 and 4. In Figure 3, signal electrons from the specimen are accelerated toward the single-crystal yttrium aluminium garnet (YAG) detector (Autrata, 1989) at ground potential and collimated near to the optical axis, so that the opening in the detector has to be small. The YAG crystal is coated with InO_2+SnO_2 and serves also as the anode of the cathode lens. The hole diameter is 300 mm in our design and the anode/detector even operates also as a movable aperture. In Figure 4, another version is shown, utilising the

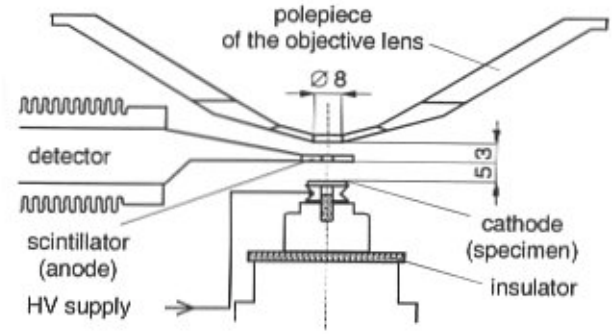

Figure 3. The adaptation of the classical SEM to the SLEEM by using the cathode lens, with the detector based on a coaxially bored YAG crystal scintillator.

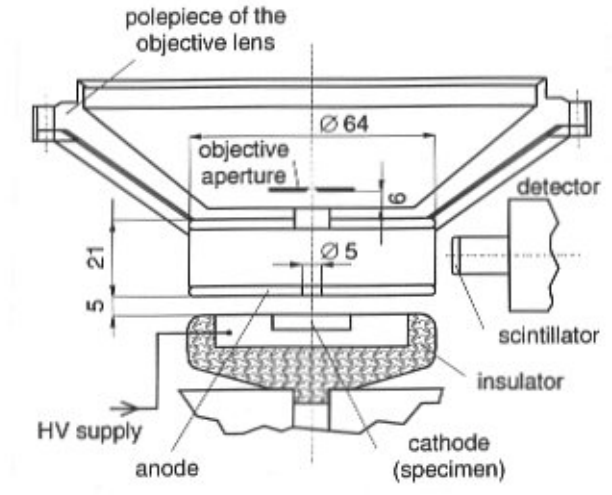

Figure 4. The adaptation of a classical SEM to SLEEM by using the cathode lens, with the detector based on a conventional Everhart-Thornley detector acquiring the tertiary electrons from the objective aperture.

---

traditional Everhart-Thornley detector. The accelerated and collimated electrons impact the objective aperture, and slow secondary ("tertiary") electrons emitted from it are attracted with a (weak) transversal field towards the side-positioned detector. The former version is more expensive and usually restricts the lowest available magnification, but it produces a very high signal, it is compact and easily adjustable as the upper detector surface is well visible so that the central bore can be aligned to the axis. The latter version brings a lower signal and takes up a larger fraction of the working distance but it is very easy to realise.

To have a small spot size of a sufficient current at low primary beam energies, we need to have a source of electrons of high brightness, as is obvious from Equations (1)

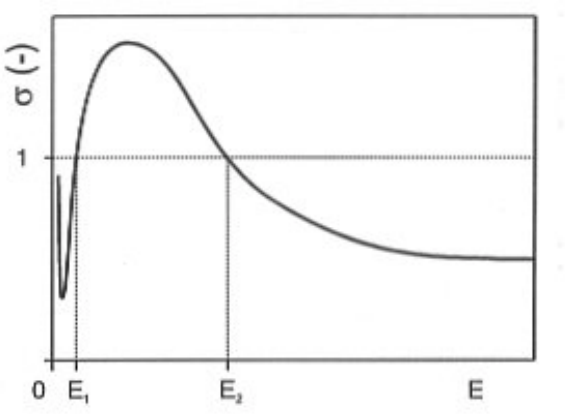

Figure 5. The total electron yield from the specimen *s* (*s*=*h*+*d*) as a function of energy.

and (2). The thermoemission (TE) cathode LaB_6 has a source brightness *B* of about $8x10^4$ A/cm^{2}sr at 5 keV while the field emission (FE) gun (Schottky emission ZrO/W<100>) has a source brightness of about three orders of magnitude higher at the same energy and the energy spread, at the cathode held at 1800 K, is *DE*=0.4 eV (Swanson and Schwind, 1997). As experience has shown, the signal level gain is so high owing to the favourable cathode lens action in collimating the emitted electrons that even with the ordinary tungsten TE gun one gets an excellent signal-to-noise ratio (SNR) in the image, while for the LVSEM, an FE gun is unavoidable. Nevertheless, if the ultimate resolution is to be reached, the FE gun is necessary even for the SLEEM, in order to secure a minimum possible energy spread *DE*. This quantity acts in the ratio, *DE/E,* to the mean energy of the electron beam so that at low energies its influence is significantly enhanced - the ultimate resolution is chromatic aberration limited.

General Trends in SEM Imaging at Low Energies

The SE and BSE signals are the ones most often used for imaging in SEM. The values of the BSE coefficient *h* and of the SE yield *d* depend particularly on the energy *E* of the electrons, mean atomic number *Z* of the specimen and angle *f* between the primary beam and the surface normal. The detector acceptance selectivity can also play a role, particularly for BSE. The dependencies are well known and proved at energies above several keV. The BSE yield *h* hardly changes as a function of *E* but it increases monotonously with *Z* and *f*. The SE yield *d* exhibits, as a function of the atomic number, some modulation reflecting the periodical table with a slow increase in *Z*, it increases more rapidly with increasing *f* and significantly increases with decreasing energy *E* (Reimer and Tollkamp, 1980). The dependencies are different below several keV and they are not yet reliably known, especially below several hundreds of eV. Nevertheless, recent results not published yet have shown that *h* also exhibits at energies below 5 keV, the wave-like behaviour similar to that which was found for *d* (Zadrazil *et al*., 1997).

The most important changes at low and very low energies for the contrast formation in conventional SEM, include:

(a) The SE yield *d* almost stops its variations with impact angle *f* at energies below, say, 500 eV. Consequently, the most noticeable contrasts in the conventional SEM, the contrasts of differently inclined facets and the edge enhancements, disappear at low energies. The reason is that the electron penetration depth no longer exceeds the SE escape depth and all SE generated can be emitted.

(b) The material contrast, traditionally acquired as the direct proportionality of the BSE signal to the mean atomic number, is no longer easy to interpret. For a couple of different *Z* materials, the mutual contrast can change its sign even several times, when going below a few hundreds eV; for elastic BSE it was clearly demonstrated by Schmid *et al*. (1983).

(c) The total electron yield *s* (*s* =*h*+*d*) behaves as shown schematically in Figure 5. *s*(*E*) increases with decreasing energy so that the charging-up phenomena get weaker and the detected signal increases because, owing to the collimating action of the cathode lens, the detected signal is closely similar to *s*.

(d) The signal of the backscattered electrons dominates at low energies, as the energy is no longer sufficient for SE production. At very low energies, the elastic BSE become the most important signal contribution.

(e) The diminished interaction volume starts to approach the dimensions of the usual “flat” relief details on most technical materials and many biological structures. Consequently, many micrographs look sharper and more rich in details at low energies although the real resolution always decreases at least somewhat.

The above mentioned properties influence the SEM imaging in the low keV range of the LVSEM and LESEM. It is expected that the tiny relief details like protrusions and ridges are much better visualised and dominate above the usually observed overbrightened edges and the facet contrast. Furthermore, the decrease in the specimen charging-up is widely utilised to image specimens which are difficult to image at normal energies. In addition, charge preventing preparation steps can be avoided.

Important from the point of view of imaging insulators is that in a normal SEM, the following phenomenon facilitating observation appears. Within the energy range (normally between a few hundred eV and a few keV) where positive charging takes place (Fig. 5), the surface charge induced field repels the slow SE towards the surface so that

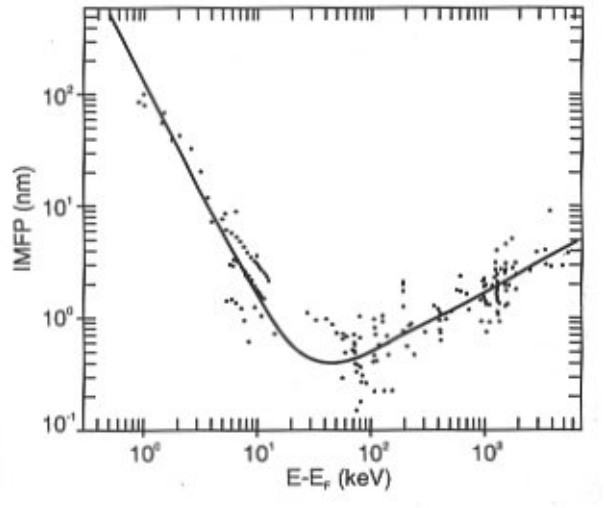

Figure 6. Compilation of IMFP measured data for elements and some compounds (dots) with the least squares fitted curve (E_F is the energy of Fermi level). Reproduced from Seah and Dench (1979).

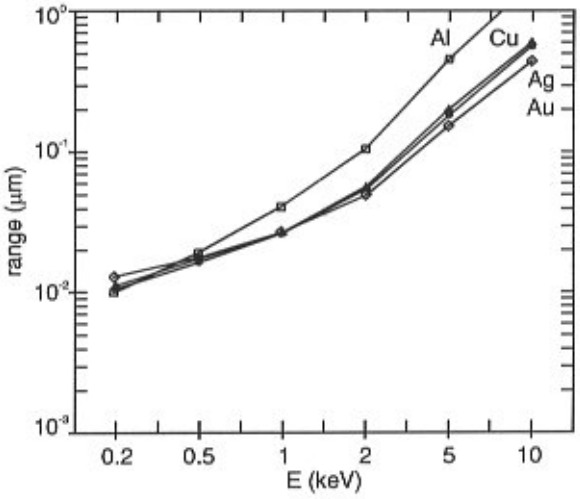

Figure 8. The computed beam range as a function of the incident electron energy for carbon, copper, silver and gold. Reproduced from Joy and Joy (1996).

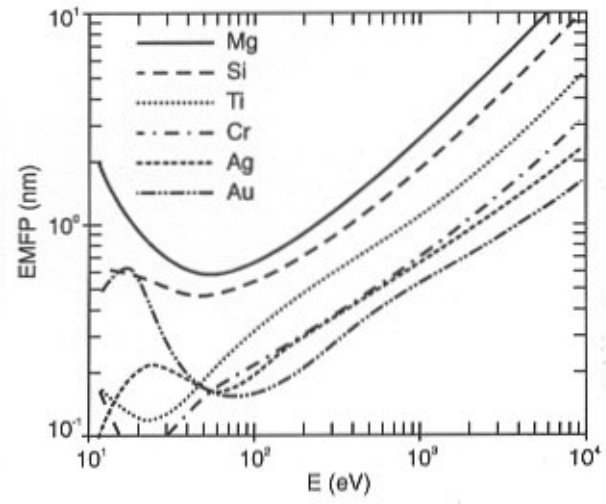

Figure 7. Calculated values of EMFP, reproduced from Ding and Shimizu (1996).

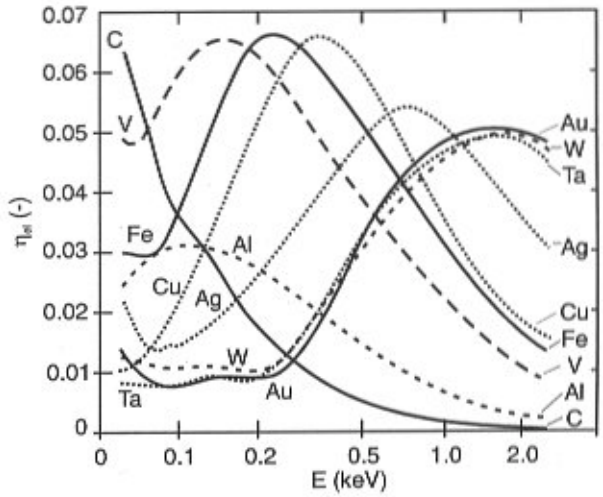

Figure 9. Backscattering coefficient h_{el} of elastically reflected electrons as a function of energy (reproduced from Schmid *et al*., 1983).

s is pushed down to unity. As the dominant SE energy is around 5 eV, even this small bias is sufficient to achieve the charge balance at which the surface potential is stabilised. Such a low surface charging allows for only slightly interfered surface imaging. This is not the case for the cathode lens where the emitted electrons are strongly extracted from the surface so that also the positive surface charge can be fully developed. This disadvantage of the SLEEM is compensated by an enhanced selection of a suitable low energy, including possibilities for the process automation (see below).

The main motivations supporting the LVSEM, LESEM and SLEEM development are the reduced charging of insulating specimens and a better transfer of high spatial frequencies in the specimen topography which, for example, improves the conditions for exact geometrical measurements on semiconductor structures by the electron beam in SEM (Maher, 1993). Nevertheless, the LVSEM and LESEM practice, as also shown below, can produce even new types of contrasts in the 100 eV range which probably cannot be reduced to (modified) traditional SEM contrasts. An en-

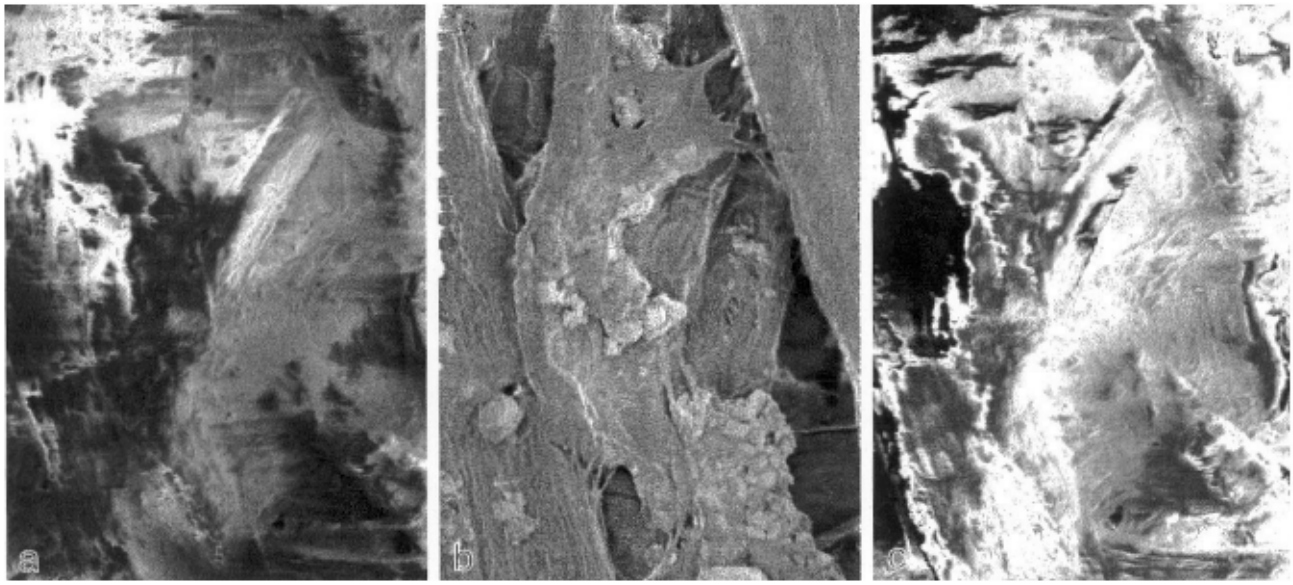

Figure 10. Surface of the writing paper, nonprocessed and uncoated, imaged at the critical energy E_2 and at energies above and below this energy. (**a**) 3650 eV, (**b**) 2650 eV (E_2), (**c**) 1850 eV, the viewfield width is 40 mm.

tirely new world of contrasts opens up in the range of tens and units of eV, which is accessible by the SLEEM. Owing to the attractiveness of this kind of microscopy, many original papers and reviews have already been published about the LVSEM and LESEM and their applications; extensive reviews have been presented by Pawley (1984) and Joy and Joy (1996). The SLEEM method has been much less widespread to date; a partial review was given by Frank *et al.* (1994). Fully relevant data obtained with slightly different instrumentation can be found in LEEM reviews like that of Bauer (1994).

Scanned Electron Imaging at Optimized Energies

We will now review the properties of the complex phenomenon of the scattering of a focused electron beam inside a solid. These indicate, in the low energy range, some features limited to a finite energy interval only. Thus, we deal with a classes of specimens that under impact of a low energy electron beam, can give rise to contrasts bound to a certain interval of the electron landing energies. First of all, we summarise the parameters describing the electron scattering which exhibit some nonmonotonous behaviour. Afterwards, we present several selected examples from the SLEEM practice, again showing contrasts appearing at some energies only, and finally we outline hypothetical explanations and propose complementary experiments to help in the image interpretations.

Electron scattering in a solid can be described on the basis of inelastic and elastic collisions, i.e. interactions between electrons and ions. The development of the Monte Carlo techniques for the scattering simulations led to progress in the formulation of the relevant theories (Joy, 1991; Ding and Shimizu, 1996). In order to facilitate both the computer simulations and the experimental verifications of important data, some quantities were defined representing certain interfaces between theory, simulation and experiment. Of these, we mention the following.

Examination of the penetration and escape depths can be based on inelastic (IMFP) and elastic (EMFP) mean free paths, respectively. A curve of IMFP is shown in Figure 6. For various elements and compounds, its values vary so little that some general dependence of IMFP on the energy can be drawn, which simplifies discussion. The curve exhibits clear absolute minimum at about 50 eV, with an increase toward higher energies and a much steeper increase downwards. This boundary divides the energy scale into two regions which can both be characterised on various bases. In connection with this, let we also look at the EMFP to energy dependence shown in Figure 7. It is plotted for several elements spanning the atomic number scale because no general curve can be fitted here. Obviously, below a similarly positioned energy threshold, the EMFP behaviour also changes but instead of starting to grow it abandons the continuous decrease and exhibits significant “modulations”. While in the higher energy region, EMFP is both longer and shorter than IMFP (depending on the atomic number), in the lower energy region, IMFP to is generally longer. In the lower range, the electron backscattering and even the elastic backscattering dominate. Around the IMFP mini-

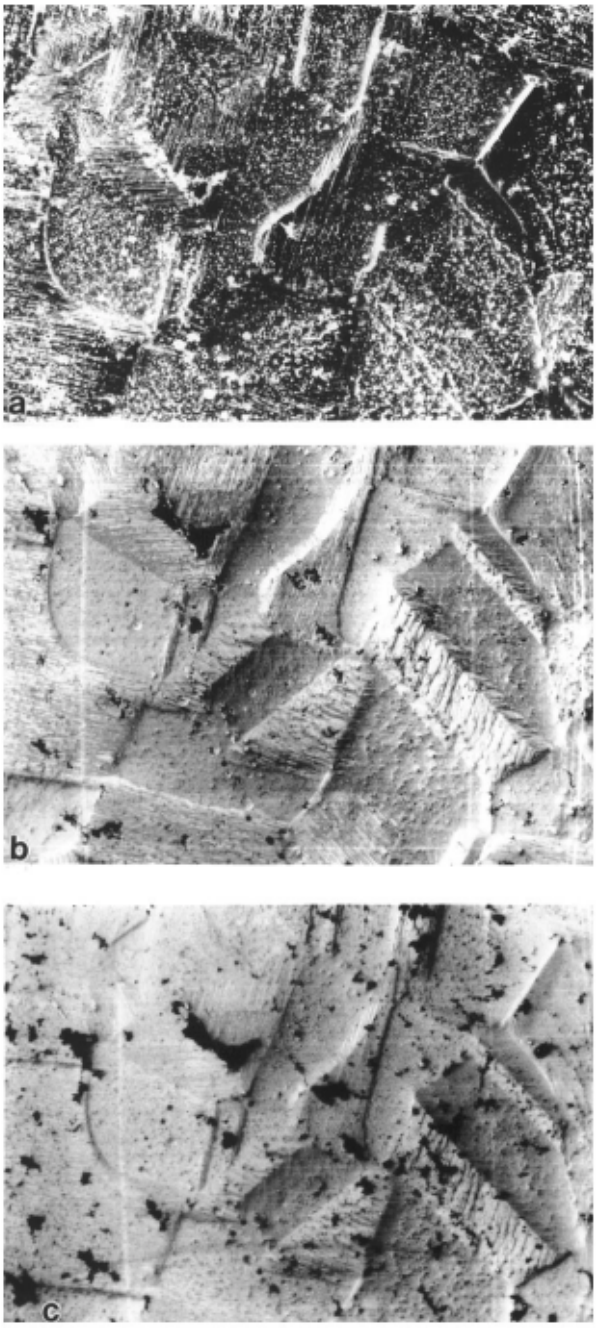

Figure 11. The pure polycrystalline Cu surface (*ex-situ* cleaned by acid etching) imaged in SLEEM. The electron energies are (**a**) 5 keV, (**b**) 200 eV, (**c**) 10 eV, the viewfield width is 100 mm.

mum, the shortest electron penetration and maximum surface sensitivity can be expected.

With regard to more phenomenological process parameters, we can mention e.g., the electron range illustrated in Figure 8, and the yield of elastic BSE in Figure 9. These

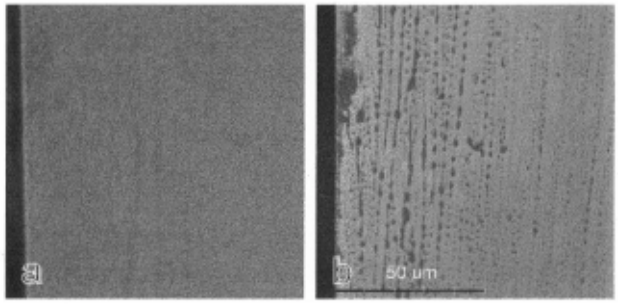

Figure 12. N^+-GaAs substrate fractured perpendicularly along an easy-to-break plane. (**a**) SE image at 10 keV, (**b**) SLEEM image at 100 eV.

data can be derived from the mean free paths and we can find them suitable for contrast interpretation. The electron range, within the energy interval shown, changes monotonously. Nevertheless, still some optimisations can take place because the maximum contrast of a particular surface relief detail can be expected when its dimensions fit those of the interaction volume. The behaviour of h_{el} corresponds to Figure 7, with the region of fluctuations beginning at a somewhat higher energy around 2 keV. But at higher energies, the portion of elastic BSE is not dominant. It is obvious that, for any pair of atomic numbers, one can find an energy at which maximum contrast in the elastic BSE signal can be obtained.

In the range of tens and units of eV, further energy optimisation opportunities emerge. Crucial is the electron diffraction producing the interference maxima within the angular distribution of the electron emission. Presence and position of the diffraction maxima for a particular local surface crystallinity is strongly electron wavelength (i.e., energy) dependent. This is the main contrast source in LEEM where in fact the low energy electron diffraction (LEED) pattern is formed in the back focal plane of the objective lens. One of the diffracted beams can be selected with an aperture and used as the signal beam so that presence of the particular crystallinity status is the image forming information. In SLEEM, the same process takes place but when using the configurations described here, the signal is collected from somewhat larger areas around the LEED patterns. Most usually, all non-specular spots are integrated on the scintillator disc or aperture (Figs. 3 and 4) or the specular beam is detected with the specimen slightly tilted (Frank and Müllerová, 1997). In both cases, significant and fast brightness changes for differently oriented crystal planes appear along the energy scale, allowing for sensitive contrast optimisations.

Another important phenomenon is the effect of the energy band structure of the specimen, i.e., of unoccupied

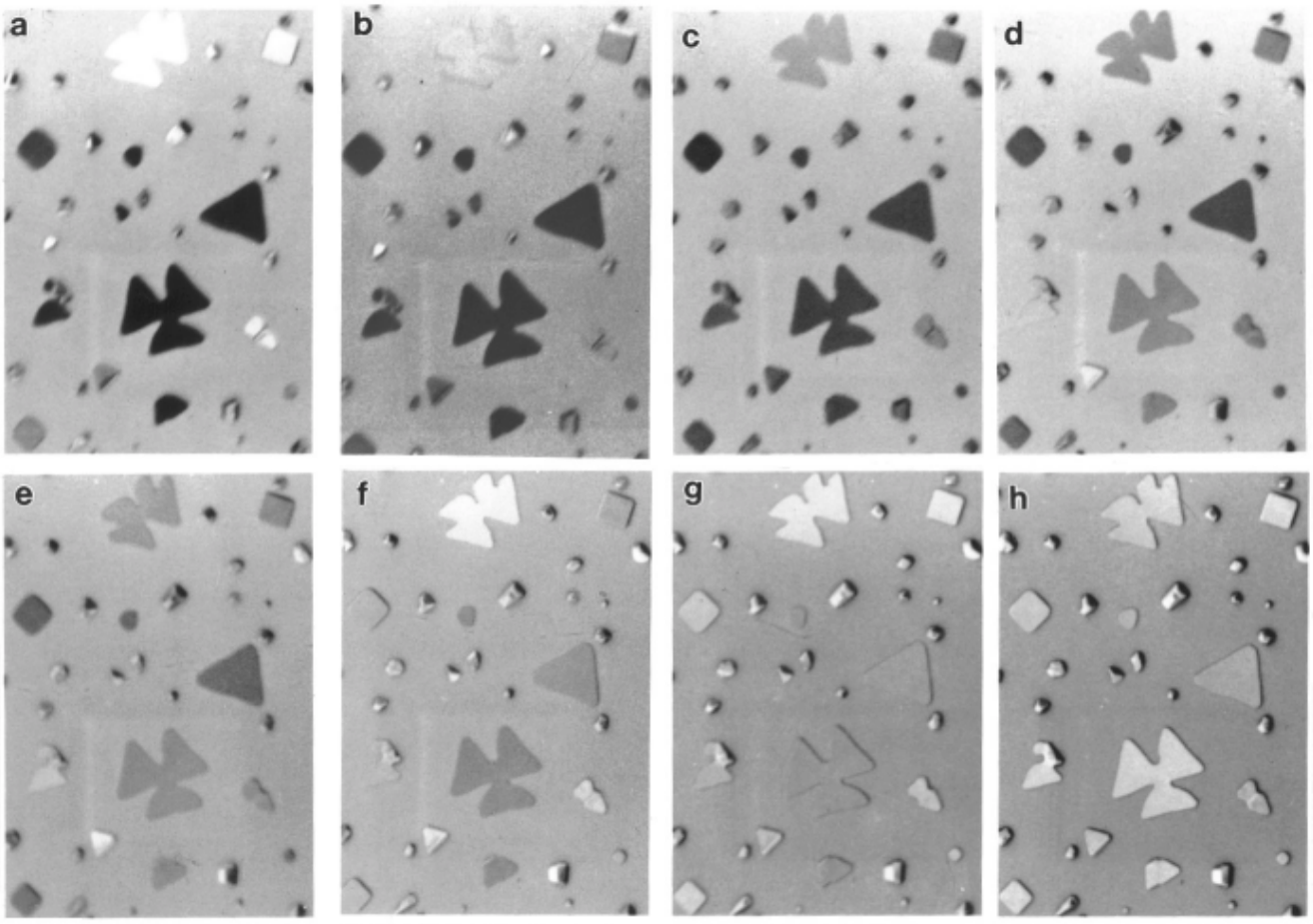

Figure 13. Flat Pb crystals of various orientations (recognisable according to the outer shape), in-situ prepared on the reconstructed Si(100)-2´1 surface, viewfield width of 30 mm, specimen tilted by 1.3°. The SLEEM energies: (**a**) 6.5 eV, (**b**) 7.5 eV, (**c**) 10.5 eV, (**d**) 16 eV, (**e**) 18 eV, (**f**) 22 eV, (**g**) 29 eV and (**h**) 34.5 eV.

bands and gaps existing above the zero energy level of the surrounding vacuum, onto the electron backscattering (see e.g., Bartoš, 1997). It appears within the landing energy range up to approx. 30 eV. Inside a specimen the impacting electron beam can be characterised by a certain wave-vector $\underline{\boldsymbol{k}}$ with respect to specimen crystal axes and by its energy increased by the inner potential. If the beam with a particular $E(\underline{\boldsymbol{k}})$ fits a forbidden gap in the $E(\underline{\boldsymbol{k}})$ pattern of the crystal, the reflection drastically increases and vice-versa. This gives rise to distinct reflectivity peaks so that again the energy optimisation of the "energy band contrast" can be made. On the other hand, the contrasts due to surface barrier variations (in height and shape) can probably appear below a certain energy but without a low energy limit.

From among additional possible contrasts sensitive to the electron energy but not obtained as yet in SLEEM, one can mention the interference contrasts on the surface atomic steps (the geometric-phase contrast) and on clusters and ultrathin films (quantum size contrast) (Bauer, 1994). These can be created by interference of the electron waves reflected either from both terraces separated by the atomic step or from both surfaces of the film; in these cases, the result is governed by relation between the electron wavelength and the step height or film thickness, respectively. The diffraction contrasts can naturally be utilised for visualisation of many processes influencing the surface crystallinity on pure or coated crystals, as extensively described by Bauer (1994).

The following examples illustrate the possible energy optimisations for the SLEEM instrument of configuration described here, i.e., without any possibility of multichannel detection of the angular emission distribution above the specimen. The experiments were partly realised under high-vacuum conditions only, which substantially extends the SLEEM application fields.

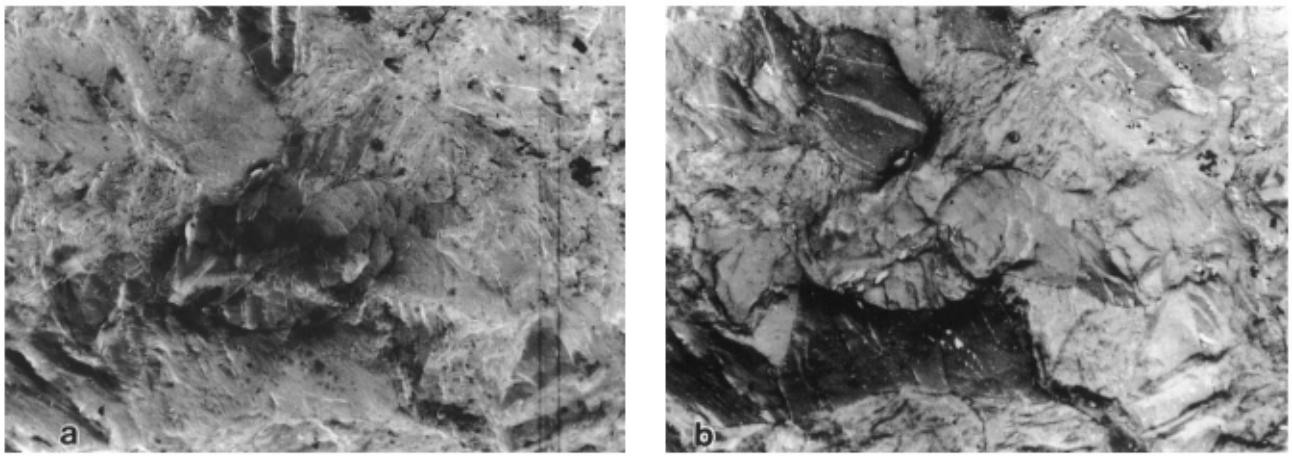

Figure 14. Polycrystalline Ti sheet, *ex-situ* cleaned by acid etching, viewfield width 50 mm. Energies for the SLEEM imaging: (**a**) 1 keV, (**b**) 50 eV.

Non-conductive specimens

At normal SEM energies, the total electron yield s is far below unity (Fig. 5) so that a good deal of the incoming charge is dissipated inside the specimen. In the case of a nonconductor, the charge stays at the surface and its field affects both the incoming and outgoing electrons so that the image is usually destroyed. As mentioned above, within the energy range where a positive charge develops, i.e., between the energy values where the $s(E)$ curve crosses the unity level, a slight charging appears amounting to only few volts (Reimer *et al*., 1992). On the other hand, in cathode lens equipped instruments a positive charging also appears so that the successful imaging is only possible at the critical energies of $s = 1$.

The energy optimisation is rather sophisticated in this case while the critical energies are not known exactly, as they are strongly specimen dependent. One possibility is to use a trial method in which some beam energy is adjusted, the beam is directed to a pixel not illuminated before and time development of the pixel signal immediately starts to be registered. When it is made for a span of energies, search for an energy with minimum signal change leads toward the higher energy of the critical ones (Frank *et al*., 1996). An example in Figure 10 demonstrates the method: Figure 10b is taken at the critical energy so that no significant charging appears. Images taken at both lower and higher energies, Figures 10a and 10c exhibit heavy charging, producing mutually reversed artificial contrasts and deformations.

This optimisation method seems to have been proved in practice and even possibilities of its automation are being tested.

Islands of heterogeneity or contamination

The very first through-energy image series taken in SLEEM, made with most easily accessible specimens like polycrystalline metal sheets (Müllerová and Frank, 1993), already showed interesting contrast changes, although the experiments were made under routine vacuum conditions. Even these easy-to-obtain micrographs reveal some simple possibilities of the surface diagnostics. One example is given in Figure 11.

Most pronounced are black areas appearing around 10 eV and nearly disappearing elsewhere. This phenomenon was frequently verified with various similarly badly defined metal specimens. One would naturally expect that the black areas show residual contamination islands not removed during the *ex-situ* surface cleaning by an acid. The contrast mechanism responsible has not been reliably explained as yet. Because the maximum contrast is obtained in the region of highly dominating elastic backscattering, one alternative is the "energy band contrast" mentioned above. However, some doubts arise because the energy of the maximum contrast is very similar for various metals and some parts of the islands are also visible at higher energies. Although both of these objections can easily be met (arguments are possible similarities in composition of contaminants on various specimens and variations in the island thickness), some complementary experiments incorporating Auger or photoelectron microanalysis are needed.

A possible application of this kind of surface diagnostics can be found not only in surface cleanliness verification but also in many tasks dealing with laterally heterogeneously coated surfaces (e.g., in the field of corrosion, catalysis, etc.) where the enhanced contrast at optimised energy can be of use.

Single-crystal surfaces

It is well known that clean surfaces of various semiconductor substrates, which are expected to be of single-

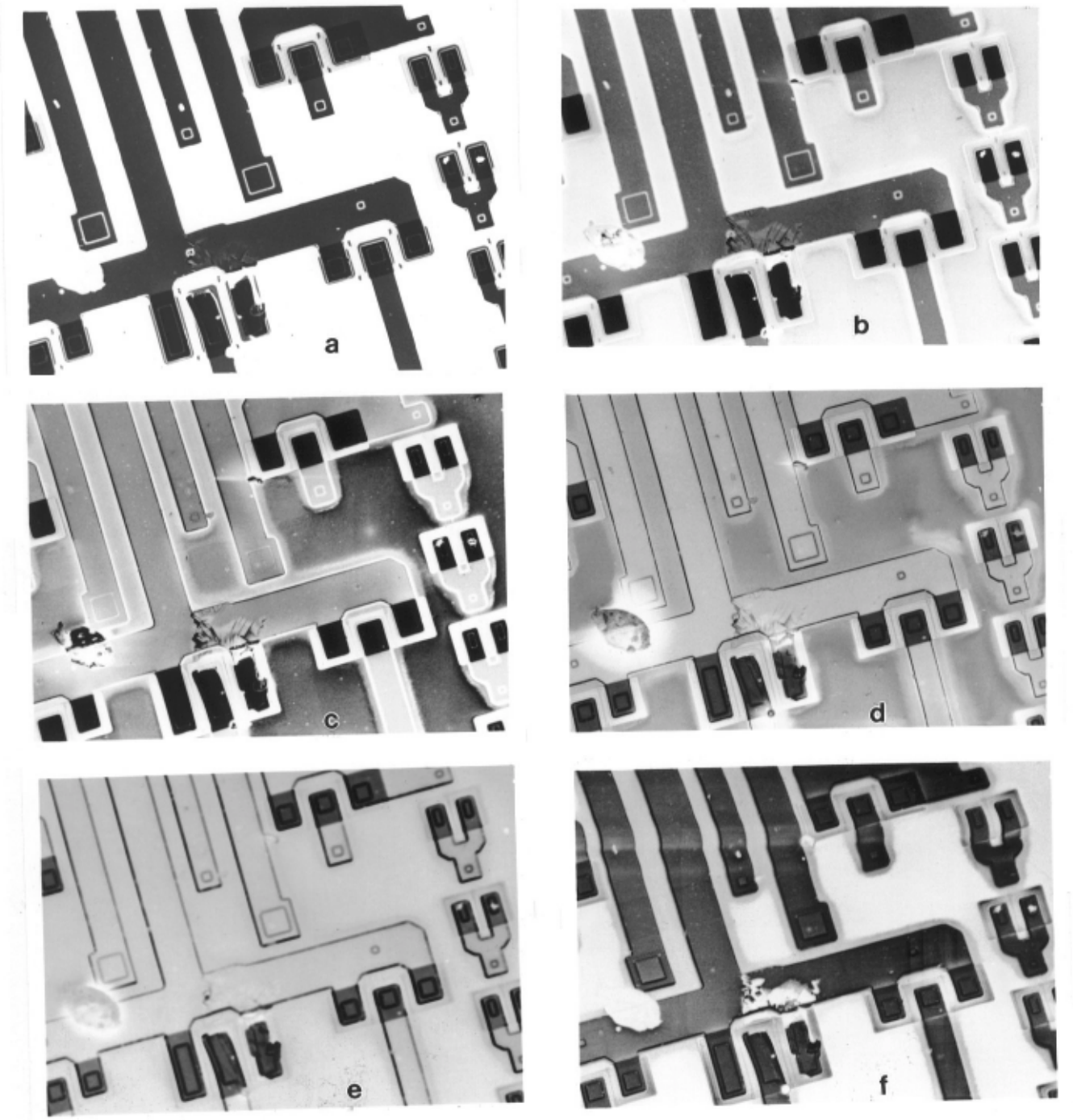

Figure 15. Surface of a GaAs technology circuit, viewfield width 400 mm. Energies for the SLEEM imaging: (**a**) 9.8 keV, (**b**) 4.8 keV, (**c**) 1350 eV, (**d**) 350 eV, (**e**) 250 eV, (**f**) 70 eV.

crystal character, exhibit hardly any contrast in the SEM under normal conditions, and are difficult to image. Nevertheless, in the range of hundreds of eV, the situation changes. Suppose the semiconductor substrate (whether Si or $A_{III}B_{V}$) is cleaned by a method usually used in device production and is for a short time exposed to the environment before it is put into the SLEEM with high-vacuum conditions in the chamber. In this case, one can observe some contrasts below say 500 eV. They appear as dark lines, dots and strips, demarcating and framing smaller contrast-less areas, mostly of extended rectangular shapes.

Analogous effects are observed on perpendicular sec-

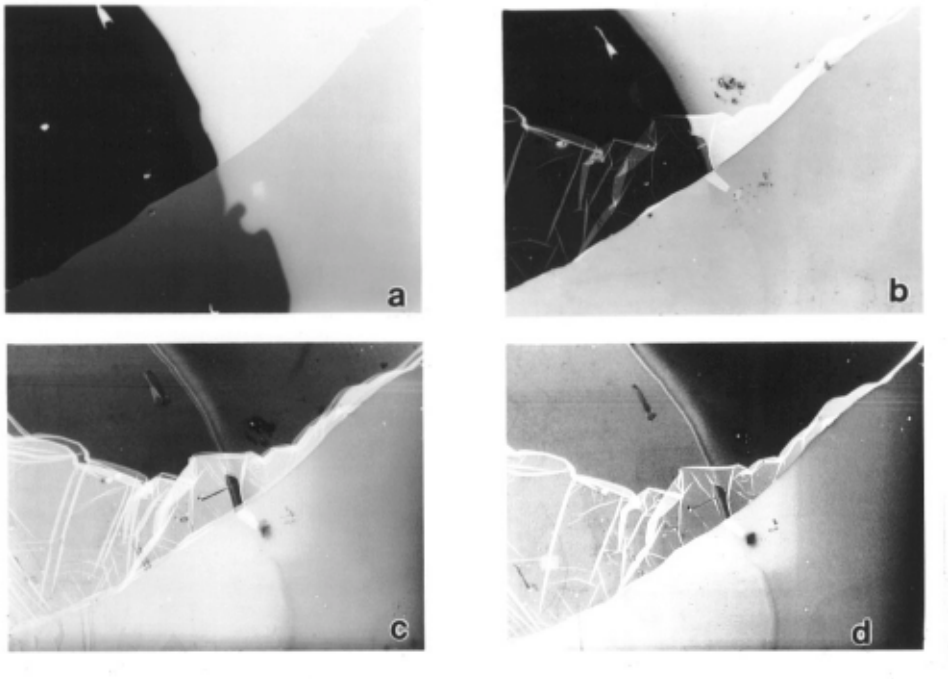

Figure l6. Specimen prepared for testing a correction algorithm for SAM: circular island of 300 nm Au layer (right) on Si substrate, crossed by the margin of the 200 nm thick GeSi layer (top left) (El Gomati *et al*., 1997), viewfield width 300 mm, reversed signal scale. Energies for the SLEEM imaging: (**a**) 9.8 keV, (**b**) 5 keV, (**c**) 850 eV, (**d**) 340 eV.

tions of the substrates, made by careful fracturing along the easy-to-break planes (Fig. 12). In this case, the prevailing features are small round dots distributed in rows, mostly parallel to the original specimen surface. The dots are in their majority of submicrometer sizes but sometimes, mainly near to the original surface, larger dots appear or the dot rows fuse into strips. The dot contrast is usually best around 100 eV but the optimum energy value is rather fuzzy.

With regard to specimen preparation, one can easily realise that on both the crystal and fracture surfaces, some initial stage of oxidation is present and observed. If we accept the idea that the oxidation occurs first and at the beginning proceeds fastest on the crystal defects of virtually all kinds, we can see in the details observed the oxide precipitates decorating the defects. Their appearance, different in the substrate plane and in the normal fracture, corresponds to the crystal growth conditions. The dot contrast, according to the energy at which it is observed, can be understood as the material contrast that exhibits some maximum for the given pair of materials. Again, before studying the phenomenon more in detail, one has to verify the chemical composition of the dots with the help of the Auger or photoelectron microanalysis.

A possible application of this type of SLEEM imaging to the semiconductor material diagnostics is straightforward. High contrast visualisation of the crystal defects can be of use in many respects.

Local surface crystallinity

The most promising SLEEM application is surely in the field of diffraction and other wave-optical contrasts. This mode of operation is naturally the most difficult because it needs true UHV conditions and specimen treatments as in a LEED apparatus. In SLEEM with single-detector configuration described here, the information channel is rather narrow: the signal is taken integrally from, for example, all nonspecular spots. Thus, it is not possible to read the local crystal orientation directly from the image - such operation mode requires using a multichannel position sensitive detector acquiring the LEED pattern. Nevertheless, as demonstrated in Figure 13, the energy optimisation for getting high contrasts between points of different crystallinity status is extremely effective. In the example shown in this figure (Frank *et al*., 1999), the specimen was slightly tilted so that the primary electron beam impacts the surface obliquely at an angle sharply increasing with decreasing energy. In this case, a high contrast can arise even between flat crystals of the same orientation but mutually rotated by a few degrees.

Diffraction contrasts cannot be passed unnoticed in this review, because they are crucial for SLEEM and they represent an excellent example of energy optimised imaging, but we will not deal with them in detail here as they are marginal to the scope of the paper.

Grains in a polycrystalline specimen

As already presented in the section on “Islands of heterogeneity or contamination”, very interesting observations can be made even with a mere *ex-situ* cleaned polycrystalline metal sheet. With some differences among various metals, somewhere at energies of 50 to 200 eV, the planar contrast between different grains reaches its maximum. This is visible in Figure 11 for Cu and also in Figure 14 for Ti. Again, it is not possible to determine the grain orientation, but contrast correlation with the grain boundaries is obvious. The

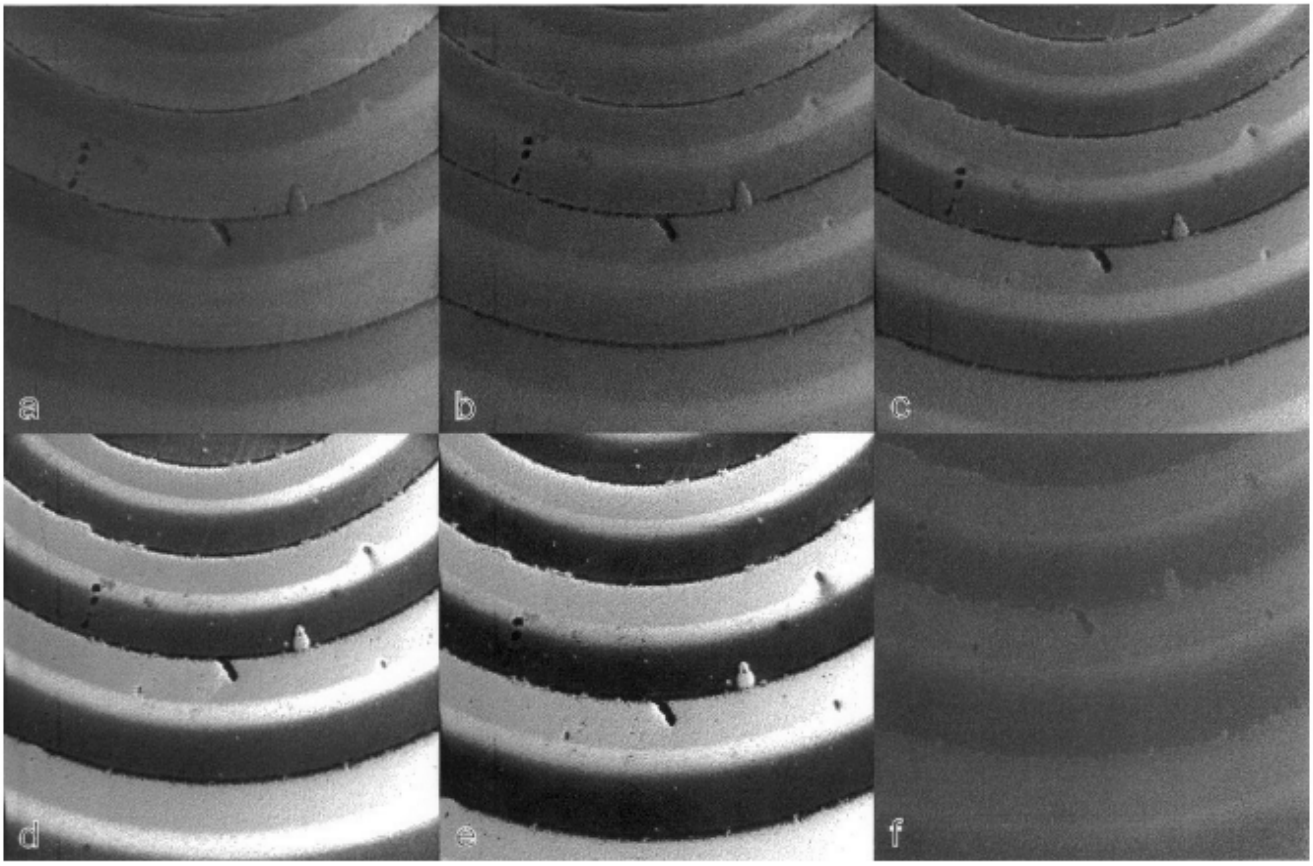

Figure 17. Bevelled cross-section made by ion beam cratering structure of couples of 100 nm GaAs / 63 nm AlAs MBE produced layers. Viewfield width 600 mm, energies for SLEEM imaging: (**a**) 20 eV, (**b**) 30 eV, (**c**) 40 eV, (**d**) 130 eV, (**e**) 430 eV, (**f**) 2430 eV.

images presented here were made both under high vacuum and UHV conditions but the specimen were not cleaned *in-situ*.

In order to determine the contrast origin reliably, one has to repeat the experiment with a polycrystal, cleaned *in-situ* by ion beam bombardment. This might support one possible explanation of the grain contrast, i.e., that it is connected with the minimum of the penetration depth where differently thin (few nm) oxide layers can produce different SE signals. Alternatively, the BSE yield variations with the crystal orientation can be responsible.

A high grain contrast, when completed by adding the orientation information, can be of use in material science in general and it could provide an alternative to the EBSP (Electron Back Scattered Patterns) mode (Dingley, 1981).

Semiconductor devices

Examination of semiconductor devices in SEM at various energies is very popular and is a common example of utilising the energy variations for a kind of non-destructive in-depth examination (Postek *et al*., 1988). The contrast depends primarily on the penetration depth, which projects itself into the BSE signal variations for the layers met within this depth. Obviously, for each layer, some optimum energy interval exists which ensures maximum contrast of a structure shaped from this layer (Rickerby, 1994). Low electron energies extend the range of this method down to the thinnest layers and, as shown in Figure 15, surface scratches and imperfections are well visible.

In the area of semiconductor technology, slow electron microscopies are extremely important for easy interoperation checks for local surface defects and also for accurate dimension measurements.

Surface coatings

Although the previous paragraph covers the layered structures most frequently used in technologies, many other examples can be found where some in-depth examination is desired. Structures discussed here can be characterised as made from mutually overlapped islands of various layers. As in the preceding example, the energy optimisation is oriented to vary the penetration depth, in order to get a contrast from the individual layers due to BSE variations and also variations in the SE yield excited by BSE (so called

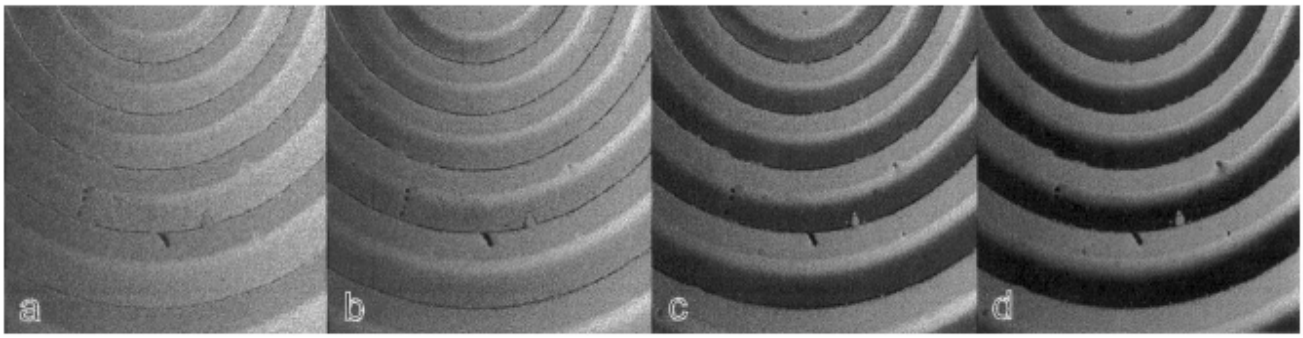

Figure 18. The dependence of the contrast shown in Figure 17 on the electron dose. Electron energy 450 eV, viewfield width 900 mm, primary beam current 0.2 nA, frame times: (**a**) 3 sec, (**b**) 11 sec, (**c**) 30 sec, (**d**) 83 sec.

SE2 signal).

A demonstration example is shown in Figure 16. The specimen used was prepared for testing a novel method for the correction of the backscattering contrast in Scanning Auger Microscopy (SAM) (El Gomati *et al*., 1992). A correct surface analysis, unaffected by the subsurface structure, can be found in SAM but not before sophisticated signal manipulations supported by complementary image signals are made. The SLEEM image series obviously provides an easy understanding of the structure so that it is a suitable complementary method to SAM.

Bevelled cross-sections of multilayered structures

Modern semiconductor devices, for example structures dedicated to fast optical communications, and X-ray optical elements are examples of technological structures containing many (even up to hundreds of) thin layers of thicknesses down to 1 nm. The structures are prepared by various types of epitaxies, very often the Molecular Beam Epitaxy (MBE) method, producing single-crystal layers. As a rule, the quality of the layer interfaces, i.e., their sharpness, is crucial for the device parameters. For this reason, observation of multilayers represents an important task for various electron microscopies. After completing a difficult preparation procedure, thin perpendicular cross-sections are observed in the transmission electron microscope (TEM) but for SEM examinations, bevelled cross-sections are necessary in order to fit the resolution range available. Bevels are made either by low energy ion beam cratering at rotation or by wet etching in a movable bath.

The final example in the series concerns the findings made on the bevels in SLEEM at low energies (Müllerová *et al*., 1997). As shown in Figure 17, within some optimum energy interval, a high layer contrast is observed on the ion-beam-cratered bevels. Surprisingly, three distinct strips per period are visible although the structure originally consists of layer couples. Within one of the strips, demarcated with sharp margins, one more rather smeared interface appears. Consequently, one interface is imaged with a very high contrast, which is extremely important for interface quality evaluations. Surprisingly, the contrast is conditioned by a sufficient electron dose, as evidenced in Figure 18, although no apparent traces of surface charging-up were noticed. Finally, the effect does not appear on wet-etched bevels, as shown in Figure 19. The peculiar contrast was observed also on other MBE manufactured multilayers, e.g., on Mo/Si mirror for X-rays.

This is a typical SLEEM observation not reliably explained as yet. Further experiments, made in an UHV SLEEM and by using complementary methods (e.g., to detect a possible very slight charging), are necessary. The only hypothesis available now is based on the assumed different extent of layer amorphisation due to the ion beam impact but the experimental data are far from being entirely explained.

Conclusions

The collection of SLEEM applications presented here to illustrate the optimised-energy microscopical approach leaves many questions unanswered. Low and very low energy microscopy can produce data so strongly encoded, as it is the case with some experimentally difficult surface examination methods like SAM. Traditional surface examination techniques are far from being routine affairs and the study of a single specimen can often take weeks. This fact can be easily understood simply because of very long pumping-down times including bake-out. Nevertheless, in SLEEM, particularly under high-vacuum conditions, a lot of surface data can be acquired quite routinely. The period of experience collection is still too short so that many easy-to-receive observations are not explained as yet, and at least for several typical specimens, each of the new contrast classes has to be studied in combination with more sophisticated surface examination tools. After necessary "calibration" with the help of external data, many of these contrast classes can serve very efficiently in practice.

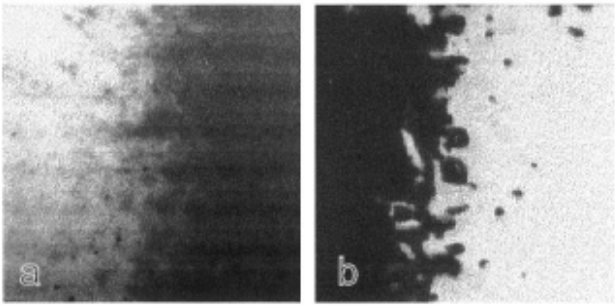

Figure 19. $In_{0.52}Ga_{0.27}Al_{0.21}As$ / $In_{0.53}Ga_{0.47}As$ interface, bevelled by wet etching in a movable bath (**a**) compared with the magnified AlAs / GaAs interface from Figure 17 (**b**). Viewfield width 25 mm, energies for SLEEM imaging: (**a**) 500 eV, (**b**) 50 eV.

Acknowledgements

This work was supported by the Grant Agency of AS CR under no. A2065502 and the Grant Agency of the Czech Republic under no. 202/95/0280 and no. 202/96/0961. The author is indebted to her co-workers L. Frank and M. Zadrazil for extensive co-operation on the projects mentioned, and to R. Steklý for the valuable help with the preparation of the manuscript.

References

Autrata R (1989) Backscattered electron imaging using single crystal scintillator detector. Scanning Microsc **3**: 739-763.

Bartoš I (1997) Electron structure of crystals from VLEED. In: Proc New Trends in Surface Analysis. Breza J, Liday J, Frank L, Král J, Zemek J (eds). Slovak University of Technology Bratislava, Slovakia. pp 39-42.

Bauer E (1994) Low energy electron microscopy. Rep Prog Phys **57**: 895-938.

Beck S, Plies E, Schiebel B (1995) Low-voltage probe forming columns for electrons. Nucl Instr Methods Physics Res **A 363**: 31-42.

Ding Z-J, Shimizu R (1996) A Monte Carlo modeling of electron interaction with solids including cascade secondary electron production. Scanning **18**: 92-113.

Dingley D (1981) A comparison of diffraction techniques in the SEM. Scanning Electron Microscopy 1981; IV: 273-286.

El Gomati M, Barkshire I, Greenwood J, Kenny P, Roberts R, Prutton M (1992) Compositional imaging in scanning Auger microscopy. In: Microscopy: The Key Research Tool. Lyman CE, Peachey LD, Fisher RM (eds). Electron Microsc Soc Am, Woods Hole. pp 29-38.

El Gomati M, Müllerová I, Frank L (1997) Combination of scanning Auger and very low energy electron microscopy. In: Proc International Centennial Symposium on the Electron. Kirkland A, Brown PD (eds). The University Press, Cambridge. pp 326-333.

Frank L (1996a) Real image resolution of SEM and low-energy SEM and its optimisation: distribution width of the total surface emission. Ultramicroscopy **62**: 261-269.

Frank L (1996b) Width of the SEM and LESEM response function as a tool for the image resolution assessment. In: Proc IX Conference on Electron Microscopy of Solids. Czyrska-Filemonowicz A, Garbarz B, Adrian H, Wojtas J, Zielinska-Lipiec A (eds). Fotobit, Krakow. pp. 109-112.

Frank L, Müllerová I (1997) Wave-optical contrasts in SEM. In: Proc 3rd Multinational Congress on Electron Microscopy. Ceh M (ed). Jozef Stefan Institute, Ljubljana, Slovenia. pp. 283-284.

Frank L, Müllerová I, Delong A (1994) Microscopy with slow electrons. Czech J Phys **44**:195-238.

Frank L, Zadrazil M, Müllerová I (1996) Low energy imaging of nonconductive surfaces in SEM. Mikrochim Acta [Suppl] **13**: 289-298.

Frank L, Müllerova I, Faulian K, Bauer E (1999) The scanning low-energy electron microscope: first attainmant of diffraction contrast in the scanning electron microscope. Scanning **21**: 1-13.

Frosien J, Plies E, Anger K (1989) Compound magnetic and electrostatic lenses for low-voltage applications. J Vac Sci Technol **B7**: 1874-1877.

Joy DC (1991) An introduction to Monte Carlo simulations. Scanning Microsc **5**: 329-337.

Joy DC, Joy CS (1996) Low voltage scanning electron microscopy. Micron **27**: 247-263.

Knoll M (1935) Charging potential and secondary emission of bodies under electron irradiation (in German). Z Tech Phys **16**: 467-475.

Lenc M, Müllerová I (1992a) Electron optical properties of a cathode lens. Ultramicroscopy **41**: 411-417.

Lenc M, Müllerová I (1992b) Optical properties and axial aberration coefficients of the cathode lens in combination with a focusing lens. Ultramicroscopy **45**: 159-162.

Maher KS (1993) Techniques for low voltage scanning electron microscopy linewidth measurements. Scanning Microsc **7**: 65-86.

Martin JP, Weimer E, Frosien J, Lanio S (1994) Ultrahigh resolution SEM - a new approach. Microsc & Anal (USA), No. 28, March 1994: 43.

Möllenstedt G, Lenz F (1963) Electron emission microscopy. In: Advances in Electronics and Electron Physics, vol. 13. Mulvey T Sheppard CJR (eds). Academic Press, London. pp. 251-327.

Müllerová I, Frank L (1993) Very low energy microscopy in commercial SEMs. Scanning **15**: 193-201.

Müllerová I, Frank L (1994) Use of cathode lens in

scanning electron microscope for low voltage applications. Mikrochim Acta **114/115**: 389-396.

Müllerová I, Lenc M (1992a) Some approaches to low-voltage scanning electron microscopy. Ultramicroscopy **41**: 399-410.

Müllerová I, Lenc M (1992b) The scanning very-low energy electron microscope (SVLEEM). Mikrochim Acta [Suppl] **12**: 173-177.

Müllerová I, Zadrazil M, Frank L (1997) Low-energy SEM imaging of bevelled multilayers. In: Proc 3rd Multinational Congress on Electron Microscopy. Ceh M (ed). Jozef Stefan Institute, Ljubljana, Slovenia. pp. 297-298.

Pawley J (1984) Low voltage scanning electron microscopy. J Microsc **136**: 45-68.

Plies E (1994) Electron optics of low-voltage electron beam testing and inspection. Part I: Simulation Tools. In: Advances in Optical and Electron Microscopy, vol. 13. Mulvey T, Sheppard CJR (eds). Academic Press, London. pp. 123-242.

Postek MT, Keery WJ, Larrabee RD (1988) The relationship between accelerating voltage and electron detection modes to linewidth measurement in a SEM. Scanning **10**: 10-18.

Reimer L, Tollkamp C (1980) Measuring the backscattering coefficient and secondary electron yield inside a scanning electron microscope. Scanning **3**: 35-39.

Reimer L, Golla U, Böngeler R, Kässens M Schindler B, Senkel R (1992) Charging of bulk specimens, insulating layers and free-supporting films in scanning electron microscopy. Optik **92**: 14-22.

Rickerby DG (1994) Low voltage field emission SEM and microanalysis of multilayer films. Eur Microsc & Anal, Jan 1994: 9-11.

Seah MP, Dench WA (1979) Quantitative electron spectroscopy of surfaces: A standard data base for electron inelastic mean free paths in solids. Surf Interface Anal **1**: 1-11.

Schmid R, Gaukler KH, Seiler H (1983) Measurement of elastically reflected electrons (E<2.5 keV) for imaging of surfaces in a simple ultra high vacuum scanning electron microscope. Scanning Electron Microscopy **1983/II**: 501-509.

Swanson LW, Schwind GA (1997) A review of the Zr0/W Schottky cathode. In: Handbook of Charged Particle Optics. Orloff J (ed). CRC Press, Boca Raton. pp. 77-102.

Thornley RFM (1960) Recent developments in scanning electron microscopy. In: Proc European Conf Electron Microsc. Houwink AL, Spit BJ (eds). Nederlandse Vereniging voor Elektronenmicroscopie, Delft. pp. 173-176.

Zadrazil M, El Gomati M, Walker A (1997) Measurements of very low energy secondary and backscattered electron coefficients. In: Proc 3rd Multinational Congress on Electron Microsc. Ceh M (ed). Jozef Stefan Institute, Ljublana, Slovenia. pp. 301-302.